Ab initio study of H-vacancy interactions in fcc metals: Implications for the formation of superabundant vacancies

R. Nazarov*
Max-Planck-Institut für Eisenforschung GmbH, D-40237, Düsseldorf, Germany
and Lawrence Livermore National Laboratory, Livermore, California 94550, USA

T. Hickel and J. Neugebauer
Max-Planck-Institut für Eisenforschung GmbH, D-40237, Düsseldorf, Germany
(Received 30 August 2013; revised manuscript received 10 January 2014; published 16 April 2014)

Hydrogen solubility and interaction with vacancies and divacancies are investigated in 12 fcc metals by density functional theory. We show that in all studied fcc metals, vacancies trap H very efficiently and multiple H trapping is possible. H is stronger trapped by divacancies and even stronger by surfaces. We derive a condition for the maximum number of trapped H atoms as a function of the H chemical potential. Based on this criterion, the possibility of a dramatic increase of vacancy concentration (superabundant vacancy formation) in the studied metals is discussed.

DOI: 10.1103/PhysRevB.89.144108 PACS number(s): 61.72.Bb, 61.72.jd, 61.72.jj, 64.70.kd

I. INTRODUCTION

The desired or unwanted presence of hydrogen in metals is a long-standing research topic in materials science. One of the astonishing implications of this presence can be an increase of the vacancy concentration in a material by several orders of magnitude, the so-called superabundant vacancy (SAV) formation. The physical picture behind this effect is a trapping of hydrogen in vacancies, yielding an overall reduction of the vacancy energy of formation. Despite the straightforwardness of such an explanation, it took until 1993 before the SAV phenomenon was first discovered experimentally by Fukai and co-workers in Pd [1] and Ni [2]. Since then, however, it has been observed in many metallic systems such as Cu [3], Ti [4], Pd and Pd alloys [5–8], Al [9], Mn [10], Fe [10,11], Mo [12], Cr [13], Co [10], Ni [14], Ni-Fe alloy [15], Nb [16–18], some hydrogen storage alloys [19], some metal hydrides [20], and stainless steels [21,22]. There are now examples available that the concentration of vacancies can become as large as 10% and more [10,23,24]. Even vacancy-ordered phases have been detected in Pd [1,5,25–27], Mn [28], Ni [14], and Fe [29]. These high-vacancy concentrations are typically not formed immediately, but only after hydrogen loading for several hours at sufficiently high temperatures [23]. However, recent investigations [10] have shown that large concentrations of vacancies (up to 10^{-4}) can be generated at internal sources of pure metals in less than 1 s. Further, hydrogen-induced vacancy formation can be substantially promoted by deformation in mechanical loading experiments [9,30–32] or strain due to phase transformations [8,33,34].

Huge vacancy concentrations are not only an interesting phenomenon by itself, there are also various examples for a significant impact on diffusion-mediated processes: Already before the discovery of SAV, an accelerated rate of host atom diffusion in an H-rich atmosphere was detected in Pd alloys [35,36] and was called hydrogen-induced lattice migration (HILM). Nowadays, typical examples for H-enhanced self- and solute-diffusion are Nb [17] and Au in γ-Fe [37]. HILM was observed in many processes under hydrogen heat treatment: for example, in accelerated phase separation of cementite [38], Pd-Rh [2,7,36,39], Pd-Pt [40–42], La-Mg [43] and Pd-Ni [44] alloys, or in terms of an accelerated ordering of Pd-Mn [45,46], Pd-Au [47,48] alloys. An increased creep rate in a H-rich atmosphere has been found for example in electrodeposited Cu [49], in polycrystalline Pd [50], and in some stainless steels [51]. Further examples for drastically accelerated interdiffusion due to H are Cu-Ni diffusion couples [52], Ni-Nb bilayers [53], and Ni-V bilayers [54].

SAVs also increase the apparent solubility of H in several metals as, for example, in Be [55], W [56], Ni, Ti, Zr, and Pd [57,58]. Huge vacancy concentrations often become a precursor of hydrogen embrittlement [59] as it has been observed in steels and others materials [60,61]. One of the reasons for this deleterious behavior is the formation of different defects, e.g., voids [62] as in the case of Al [9], Ni [63], Fe [64,65], steels [66], and/or dislocation loops [19,21,40].

To investigate SAV formation from a theoretical point of view, one has to consider the energetics of vacancies and H interstitial atoms, including their binding energy. In addition, it is important to note that H atoms have a high number of configurations inside a vacancy, which leads to a higher configuration entropy of a crystal with H-vacancy complexes than of a crystal with empty vacancies and H in bulk interstitial positions. Therefore, a combination of *ab initio* calculations and thermodynamic concepts can be used to predict SAV formation.

We have recently suggested such an approach for the case of fcc Fe [67], providing SAV concentration as a function of temperature and H chemical potential. In this work, all relevant point defect clusters for an extensive set of fcc metals have been numerically evaluated and used for the grand canonical ensemble. This does not only include single H atoms in a vacancy, but also the possibility that at H-rich conditions a vacancy can be loaded with n H atoms. For these kinds of considerations it is, therefore, decisive to know the number of H atoms trapped in a single vacancy as function of the H chemical potential. This number is hardly accessible in

*nazarov1@llnl.gov

experiment, but can be evaluated using state-of-the-art *ab initio* calculations. Indeed, several previous theoretical works have been focused on this aspect.

First studies performed at the end of the 1980s employed an effective-medium theory (EMT) without relaxation of host atoms to consider Fe [68], Ni [69], Cu, Mo, Pd, Nb [70]. The dominant contribution to the binding energy of H with a vacancy came from a term that depends only on the average electron density around H. The first H atom optimizes its position in the vacancy according to this charge density, yielding a certain H-vacancy binding energy. The inclusion of more H atoms, however, introduces an additional charge density at the H site, which reduces the H-vacancy binding energy. This effect, which depends on the configuration of the H atoms in the vacancy, has been used by Nordlander *et al.* to explain the experimentally observed two different values of H-trapping energies [70]. Following a similar theory, Liu *et al.* [71] suggested that an empty vacancy includes an isosurface of optimal charge density for the incorporation of H atoms. By distributing H atoms onto this isosurface, they found that 10 of them can be trapped by a monovacancy of W.

H-vacancy interaction was probably studied most extensively for bcc W, due to its relevance as a first wall material in fusion reactors. In most of the recent studies, H atoms were distributed over the six available octahedral sites (OS) inside a vacancy in W, yielding a maximal occupancy of 6 H atoms per vacancy [72,73]. Ohsawa *et al.* [74], however, found that up to 12 H atoms can be trapped by a single W vacancy. The situation is similarly unclear for bcc Fe. Using density functional theory (DFT) within generalized gradient approximation (GGA), it was found [75] that up to 5 H atoms can be trapped in a single vacancy. This is in contrast to previous EMT calculations [69], in which at least six trapped H atoms were observed. Very recently, a complete study on H-vacancy interaction in bcc transition metals has appeared [76]. In contrast to the findings of Tateyama and Ohno [75], the authors have shown that up to 6 H atoms can be trapped in a single vacancy in Fe and in other bcc metals (V, Nb, Ta, and Cr). Furthermore, up to 10 and 12 H atoms can be accommodated according to their findings in a Mo and W monovacancy, respectively.

In contrast to bcc metals, the number of theoretical studies on the H trapping in fcc metals is rather limited and again characterized by deviating results. For the example of Al, Lu and Kaxiras [77] used DFT in the local density approximation (LDA) and found that up to 12 H atoms can be incorporated in a single vacancy. According to them, the H atoms are distributed in 6 H pairs, which have bond lengths of about 1 Å and are oriented along ⟨100⟩ directions. One H atom in each pair is situated very close to an octahedral site (OS) inside a vacancy and the other H atom is positioned closer to the center of a vacancy. Ismer *et al.* [78] questioned the maximal H occupation in Al vacancies reported by Lu and Kaxiras. According to their DFT results based on GGA, only 10 H atoms can be trapped in a monovacancy of Al: 8 of them are located in tetrahedral sites (TS) inside a vacancy and another two form a hydrogen molecule. In their work they used a different criterion for the stability of nH-vacancy complexes than Lu and Kaxiras: According to them, only those nH-vacancy complexes can be formed, for which the reaction enthalpy of adding the nth H into an $(n-1)$H-vacancy complex is negative. Furthermore, Vekilova *et al.* [79] studied the interaction of H with vacancies in Pd in the framework of DFT using LDA. They showed that 6 H atoms can be trapped in a single vacancy and their positions are close to the OS within a vacancy. Also, in our previous study [67] on fcc Fe, we found that at least 6 H atoms can be trapped by a monovacancy. The positions of H atoms are close to OS within a vacancy.

Summarizing these findings, there is no consensus about the most suitable theoretical approach to investigate the interaction of H with vacancies. This includes aspects such as the choice of exchange-correlation functionals, the preferential position for H to consider, the possibility of formation of a second H layer inside a monovacancy and the criteria for trapping H atoms by a vacancy, and the determination of the maximum number of H atoms with which a vacancy can be loaded. Therefore, the goal of this paper is to present a systematic study of H-vacancy complexes in fcc metals. To this end, we have investigated 12 fcc metals: Ag, Al, Au, Ca, Cu, Ir, Ni, Pb, Pd, Pt, Rh, and Th. We discuss on the same footing the preferential positions for H inside a vacancy, the stability of a second H layer formation inside a monovacancy, and suitable criteria for the stability of H-vacancy complexes. As a result of these considerations, we demonstrate in this work that a large number of H atoms can be trapped in monovacancies of fcc metals and predict the conditions of superabundant vacancy formation.

II. METHODOLOGY

A. *Ab initio* approach

In this work, we have employed density functional theory [80,81] as implemented in the Vienna *Ab Initio* Simulation Package (VASP) [82–84]. We have used the GGA exchange-correlation functional of Perdew and Wang [85]. The convergence parameters were the same as in one of our previous works [86]: a 6912 k point · atoms (or finer for some hydrides) mesh and a metal-specific energy cutoff [87]. With the use of these parameters, the H solution enthalpies converged to an accuracy of better than 0.05 eV. For complete relaxation of the system, the convergence criteria enforced the forces on each atom to be below 0.01 eV/Å. The first-order Methfessel-Paxton method [88] was used for the Fermi-surface smearing. The smearing width of 0.1 eV was chosen such that the corresponding error in the 0-K extrapolated energy is less than 1 meV/atom.

With the use of the above-mentioned parameters, the lattice constants and bulk modules for all 12 studied metals as well as the magnetic properties of Ni are in good agreement with available experimental values (see Table 1 in Ref. [86]).

In order to ensure that the formation energies of point defects correspond to the dilute limit, i.e., excluding interactions with periodic images of defects, we have performed a careful convergence analysis with respect to supercell size. The results of such an analysis show that already a $2 \times 2 \times 2$ supercell with 32(31) host atoms is sufficient to achieve a precision of the vacancy formation energy of better than 0.1 eV for all metals considered here. The origin of the rapid size convergence, which is much faster than what is commonly observed for vacancies in semiconductors, are the small atomic relaxations around the vacancy in fcc metals and the highly efficient

electronic screening in metals. Therefore, all our calculations have been done in such a supercell. Consistently, we consider also all interactions that lie below our accuracy of 0.1 eV as being too small to be relevant for the results of this paper.

B. Formation energies

Every point defect (δ) changes the equilibrium structure of a crystal by the point-defect formation volume (Ω_f^δ), which can be determined in DFT calculations by

$$\Omega_f^\delta = N\Omega - (N + \Delta n_X)\Omega_0. \quad (1)$$

Here, N is the number of lattice sites in the supercell, Ω and Ω_0 are the volume per site in the supercell with and without a defect respectively, Δn_X is the difference in the number of X-host atoms between these two supercells.

The key quantity commonly used to describe the concentration of H containing defects in a metal is the defect Gibbs formation energy

$$G_f^\delta = G_f^{\delta,0} - n_H(\mu_H - \mu_H^0), \quad (2)$$

i.e., the energy needed to take n_H H atoms out of their chemical reservoir μ_H and create a defect containing n_H atoms in the metallic matrix. Such defects may be interstitial H or a vacancy loaded with H atoms. $G_f^{\delta,0}$ in expression (2) defines the Gibbs formation energy at some reference H chemical potential (μ_H^0). The resulting linear dependence is illustrated in Fig. 1 for some H-vacancy complexes, where the slope is equal to n_H, the number of H atoms in the defect.

In Fig. 1, the thermodynamically most favorable defect for a specific H chemical potential is given by the defect with the lowest formation energy G_f^δ (e.g., for vacancy-containing defects shown by the red line). As shown in Fig. 1, increasing the hydrogen chemical potential lowers the formation energy of defects containing H, whereas those free of any H (such as the unloaded vacancy) remain constant. As a consequence, above a critical H chemical potential μ_H^{SAV} the empty vacancy is

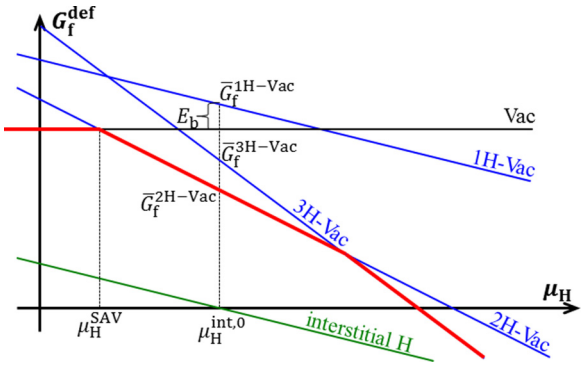

FIG. 1. (Color online) Schematic diagram introducing the key quantities/parameters used in our formalism. Shown are the Gibbs energies of formation of a vacancy (black line), of H-vacancy complexes (blue line), and of interstitial hydrogen (green line) as a function of H chemical potential. The formation energy of thermodynamically stable H-vacancy complexes is shown by the red line. μ_H^{SAV} is the H chemical potential of superabundant vacancy formation. $\mu_H^{int,0}$ is the chemical potential for which the formation energy of an interstitial H becomes zero [$G_f^{int}(\mu_H^{int,0}) = 0$]. E_b is the binding energy of a single H atom to a vacancy.

no longer the thermodynamically preferred defect but vacancy-hydrogen complexes, i.e., vacancies that are filled with one or more H atoms. This onset is the condition of superabundant vacancy formation. In the case sketched in Fig. 1, it is not the vacancy loaded with a single H atom, as may be expected, but a vacancy loaded with 2 H atoms. In fact, in the scenario shown in Fig. 1, the configuration with a single H in a vacancy never becomes thermodynamically stable.

The actual number of H atoms with which a vacancy is filled depends on the H chemical potential. The maximum filling is realized at the maximum possible H chemical potential at which the considered system is thermodynamically still stable.

The system is thermodynamically stable if the formation energy of any competing bulk phase or defect (interstitial H, H-vacancy complexes) is positive, i.e., the presence of defects is only due to configurational entropy. As can be seen from Eq. (2) at very high H chemical potential, the formation energy of any H-containing defect can become zero. This will result in a transformation into a new phase where H-containing defects will occupy all available interstitial sites (e.g., NaCl-type of hydride if $G_f^{int} = 0$ or a vacancy-ordered hydride phase if $G_f^{nH\text{-}Vac} = 0$). We note that the linear dependence on the H chemical potential shown in Eq. (2) is only valid in the dilute concentration limit. As has been discussed, e.g., by Kirchheim in the defactant concept [89], the defect formation energy shows a nonlinear behavior when the interaction energy between defects can no longer be neglected. As a consequence, the exact value of the H chemical potential at which a hydride phase forms will be shifted to smaller (larger) μ_H if the effective H-H interaction is attractive (repulsive).

Since we will show in the following that the H-H interaction yields in our systems shift that are rather modest and typically in the order of our accuracy limit of 0.1 eV, it will not explicitly be considered in this work. The absence of strong interactions can also be concluded from the fact that in contrast to most other point defects, large concentrations of up to 100% have been observed for H impurities. Although the linear extrapolation of defect Gibbs energies for interstitial H in a metallic matrix is apparently justified, we will still provide in the following the theoretical framework to calculate phase diagrams based on DFT calculations of bulk phases including pure fcc metal, NaCl types of hydrides, and other experimentally observed types of hydrides not based on a fcc structure. The phase transformation from a phase σ to a phase σ' occurs if

$$G_f^\sigma(\mu_H^{\sigma\to\sigma'}) = G_f^{\sigma'}(\mu_H^{\sigma\to\sigma'}), \quad (3)$$

where the formation energies of both phases are taken per host atom. The H chemical potential for a transformation into the first hydride phase, i.e., the value at which the system transforms from the metallic bulk phase into a hydride, determines the upper limit the H chemical potential can reach in the metallic (i.e., nonhydride) phase. The number of H atoms in a vacancy at this H chemical potential will correspond to the maximal filling of a vacancy by H in fcc metal.

In previous studies, two alternative approaches to identify the maximum filling of vacancies with H have been proposed and applied: The first criterion [74,76,77] identifies the complex with the largest number n of H atoms that is thermodynamically stable against a dissociation into an empty

vacancy and H on bulk interstitial sites:

$$G_{\mathrm{f}}^{n\text{H-Vac}} \leqslant G_{\mathrm{f}}^{\mathrm{vac}} + n_{\mathrm{H}} G_{\mathrm{f}}^{\mathrm{int}}. \tag{4}$$

Since the number of H atoms does not change in this reaction, the H chemical potential can be freely chosen. A particularly convenient choice to express relation (4) is achieved by choosing $\mu_{\mathrm{H}} = \mu_{\mathrm{H}}^{\mathrm{int},0}$ such that the formation energy of an H interstitial $G_{\mathrm{f}}^{\mathrm{int}}$ becomes zero $[G_{\mathrm{f}}^{\mathrm{int}}(\mu_{\mathrm{H}}^{\mathrm{int},0}) = 0]$. For this specific choice, relation (4) simplifies and we get

$$\bar{G}_{\mathrm{f}}^{n\text{H-Vac}} \leqslant \bar{G}_{\mathrm{f}}^{\mathrm{vac}}, \tag{5}$$

where the specific choice of the H chemical potential is marked by a bar above the corresponding Gibbs energy:

$$\bar{G}_{\mathrm{f}}^{\delta} = G_{\mathrm{f}}^{\delta}\left(\mu_{\mathrm{H}}^{\mathrm{int},0}\right), \tag{6}$$

which we will call in the following adjusted Gibbs energy of formation.

The commonly employed criterion formulated by relation (5) allows us to directly compare the energy of the complex with that of the empty vacancy. However, this criterion can yield an overestimation of the number of H atoms. For the schematic example shown in Fig. 1, the criterion would predict that the 3H-Vac complex corresponds to maximum filling. However, as shown in Fig. 1, this complex is thermodynamically unstable against the formation of a complex with 2 H atoms. What is missing in this often employed criterion is that the complex should not only be thermodynamically stable against a dissociation into a vacancy and interstitial H, but also against an incomplete dissociation into smaller H-vacancy complexes. In the grand canonical approach outlined here, all possible types of defect dissociation are included as sketched in Fig. 1.

A second popular criterion is based on a kinetic argument [72,75,78]: An additional H atom can join an existing H-vacancy complex if its Gibbs energy of formation ($G_{\mathrm{f}}^{i\text{H-Vac}}$) is lower than that of the former H-vacancy complex ($G_{\mathrm{f}}^{(i-1)\text{H-Vac}}$) and that of an interstitial H atom together:

$$G_{\mathrm{f}}^{i\text{H-Vac}} \leqslant G_{\mathrm{f}}^{(i-1)\text{H-Vac}} + G_{\mathrm{f}}^{\mathrm{int}}. \tag{7}$$

Choosing the same reference H chemical potential $\mu_{\mathrm{H}}^{\mathrm{int},0}$ as in Eq. (5), Eq. (7) simplifies to

$$\bar{G}_{\mathrm{f}}^{i\text{H-Vac}} \leqslant \bar{G}_{\mathrm{f}}^{(i-1)\text{H-Vac}} \tag{8}$$

indicating that the filling of a vacancy with H atoms stops, if the adjusted Gibbs energy of formation of possible larger H-vacancy complexes becomes higher than that of the present complex. Applying this criterion to the situation shown in Fig. 1, then no H would enter a vacancy since at $\mu_{\mathrm{H}}^{\mathrm{int},0}$ the Gibbs energy of the 1H-Vac complex is already higher than that of an empty vacancy. In the thermodynamic limit, however, the 2H-Vac complex is most stable for this H chemical potential and as can be seen in Fig. 1, even a 3H-vacancy complex can be formed at higher μ_{H}. Taking into account that H as an interstitial element is rather mobile and that vacancies are formed at higher temperatures, we expect that in most cases the thermodynamic criterion will prevail over the kinetic one.

The concept of choosing a suitable reference H chemical potential can be also used to obtain other experimentally relevant information. For example, the H-Vac binding energy, i.e., the gain in energy when an interstitial H moves to a vacancy, is often accessible in experiment:

$$E_{\mathrm{b}} = G_{\mathrm{f}}^{\mathrm{vac}} + G_{\mathrm{f}}^{\mathrm{int}} - G_{\mathrm{f}}^{1\text{H-Vac}} = \bar{G}_{\mathrm{f}}^{\mathrm{vac}} - \bar{G}_{\mathrm{f}}^{1\text{H-Vac}}. \tag{9}$$

Therefore, the binding energy is the difference between the adjusted Gibbs energy of vacancy formation and the adjusted Gibbs energy of formation of a 1H-Vac complex as shown in Fig. 1.

The thermodynamic analysis of point defects with and without hydrogen discussed above is based on the Gibbs energy of formation of point defects (or phases) and can be applied to any open system at constant temperature and pressure placed in a reservoir with constant H chemical potential (i.e., described within a grand canonical ensemble). The dependence on temperature and pressure will only result in a shift of the Gibbs energy lines in Fig. 1 and we assume that this will not affect the qualitative description given above. Therefore, the Gibbs energy of formation of any point defect can be approximated by the corresponding DFT energy computed at 0 K and zero pressure:

$$G_{\mathrm{f}}^{\delta,0} \approx E_{\mathrm{f}}^{\delta} = E_{\mathrm{tot}}^{\delta} - E_{\mathrm{tot}}^{\mathrm{bulk}} - \mu_{\mathrm{X}}^{0}\Delta n_{\mathrm{X}} - \mu_{\mathrm{H}}^{0} n_{\mathrm{H}}, \tag{10}$$

where $E_{\mathrm{tot}}^{\delta}$ and $E_{\mathrm{tot}}^{\mathrm{bulk}}$ are the total energies of a supercell with and without a defect. The reference chemical potentials of the elements are the energies per atom of the pure fcc structures ($\mu_{\mathrm{X}}^{0} = E_{\mathrm{tot}}^{\mathrm{bulk}}/N$) and of the H_2 molecule in vacuum ($\mu_{\mathrm{H}}^{0} = \frac{1}{2}E_{\mathrm{H}_2}$).

C. H positions within vacancies

The calculation of the defect formation energy in Eq. (10) requires the identification of the most preferable position for a H atom inside a vacancy. For this purpose, one in principle needs to construct the whole $3n$-dimensional potential energy surface (PES) for the incorporation of n H atoms at different positions and a subsequent determination of its minima. Such kinds of calculations are extremely expensive even if the high symmetry of the fcc structure is taken into account. Therefore, we propose here a different approach:

Due to the small size of the H atoms, the internal surface of a vacancy can, to first order, be viewed as a free metallic surface. This has the advantage that the preferential positions of H can now be determined by searching for local minima on a two-dimensional (2D) PES, similarly to concepts in surface physics [90]. In order to visualize the internal surface, we employ a stereographic projection on the plane. The center of the stereographic sphere is placed in the center of the vacancy. We then project the positions of host atoms first on the surface of the stereographic sphere and then from there onto the (001) plane using a pole of the stereographic sphere that is situated in the [001] direction. The positions of host atoms from the first shell around a vacancy together with the high-symmetry directions are shown in Fig. 2. Due to the high number of point-group-symmetry operations in fcc structure ($N_{\mathrm{sym}} = 48$), the 2D PES needs to be computed only in a $1/N_{\mathrm{sym}}$ part of the full solid angle as shown in Fig. 2. Utilizing the point-group symmetry thus provides a significant reduction of the number of calculations needed to find the most preferable places (minima on the 2D PES).

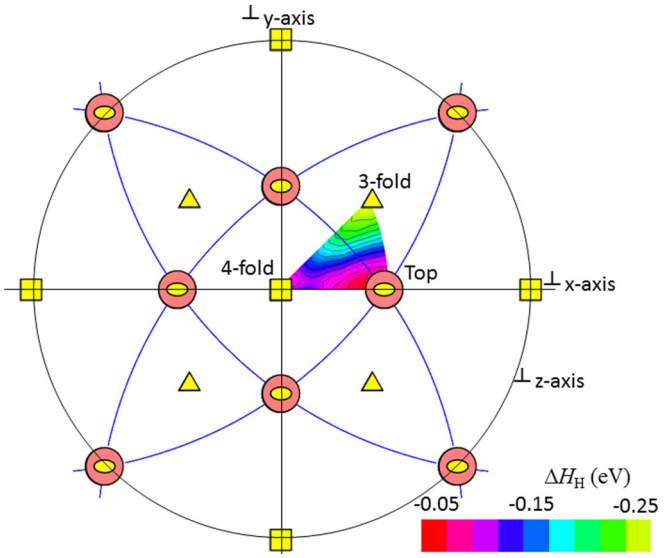

FIG. 2. (Color online) Stereographic projection of the potential energy surface (PES) of a H atom on the internal surface of a vacancy in nonmagnetic fcc Fe. Only the irreducible part of the PES is shown.

However, the situation becomes challenging when the situation of adding n H atoms to a single vacancy is considered since this would require the mapping of a $2n$-dimensional PES which is computationally not feasible.

To make the computation feasible, it is important to note that the energetic minima (or maxima) of the hydrogen PES inside a vacancy are typically situated at high-symmetry points (Fig. 2). Therefore, instead of constructing the whole PES for multiple H atoms inside a vacancy, we consider in the following the occupation of three high-symmetry sites: (i) the on-top site situated in the direction of the symmetry axes of second order ($\langle 110 \rangle$) and of host atoms in the first shell, (ii) the threefold-coordinated sites situated in the direction of the symmetry axes of the third order ($\langle 111 \rangle$) and the TS within a vacancy, and (iii) fourfold sites in the direction of the symmetry axes of the fourth order ($\langle 100 \rangle$) and of the OS within a vacancy.

As will be shown later, the internal volume of a vacancy of some fcc metals is large enough to incorporate several layers of H. When considering the multiple decoration of the vacancy internal surface with H, we assume in this work that H atoms within each layer occupy the same type of high-symmetry sites. The type of sites in a next H layer can be different from the previous one.

D. Quantum effects

When calculating solution enthalpies of light elements such as H, zero-point energies are known to yield a sizable contribution. Therefore, we computed the quantum mechanical zero-point energy of interstitial H by numerically solving the three-dimensional (or one-dimensional in the case of a H_2 molecule) Schrödinger equation. The required potential is determined by displacing the H atom from its equilibrium position in the $\langle 100 \rangle$, $\langle 110 \rangle$, and $\langle 111 \rangle$ directions and interpolating with a fourth-order polynomial to obtain an analytical expression for the local 3D PES. For the H_2 molecule, the 1D PES has been constructed by varying the distance between H atoms. Due to the large mass difference between the H atom and the host atoms, the H quantum oscillation is largely decoupled from the motion of host atoms. Therefore, we apply the adiabatic approximation keeping the positions of the host atoms frozen during the displacement of the H atom. This approximation compares well to more expensive calculations of the full dynamical matrix [91,92].

According to our calculations, the zero-point energy of a H_2 molecule in vacuum is 0.344 eV, which agrees well with the experimental value [93] of 0.372 eV. To correct the formation energies of defects containing a H atom, the difference between the zero-point energy of H in the defect and half of the zero-point energy of the H_2 molecule is added.

We find the zero-point energies for bulk interstitial sites to be very similar to those for the same type of interstitial sites inside a vacancy. As a consequence, we find that the stability of H-vacancy complexes is practically not affected by H quantum effects.

III. RESULTS AND DISCUSSION

A. H in interstitial positions

As the formation energy of interstitial H is a crucial input for the thermodynamic analysis, we discuss its computation and accuracy in detail. The computed H formation energies in the dilute limit for the two relevant types of interstitial sites (OS and TS) are for all considered elements shown in Table I together with experimental results. All calculations have been performed for H sitting in the center of the interstitial site and full lattice relaxations have been used.

In contrast to the common belief [121] that H in fcc metals prefers octahedral sites, which provide a larger interstitial volume than tetrahedral sites, our results show that H prefers the TS location in Al, Au, Ca, Pb. Furthermore, it turns out that the preferential location in an OS in Ag is only due to the higher zero-point energy contribution for H in TS compared to the OS. These findings are in agreement with experiments on Al [115], Pd [116–118], Pt [119], and with previous DFT calculations for H in Ca and Cu (see, e.g., Ref. [92]).

An additional aspect for H incorporation in OS has been observed in Au, Pb, and Pt. In these metals, the ground-state H position is not situated in the center of the OS, but displaced in the $\langle 111 \rangle$ direction (see Fig. 3) towards the trigonal position (see Fig. 4). The maximal displacement of about 0.6 Å is observed for Au, for Pb the offset is about 0.3 Å, and for Pt 0.4 Å. For TS, an off-center configuration is found only for H in Ag. The H atom is displaced from the TS center by 0.03 Å. Similarly, an instability for H in OS sites has been observed, if Zn, Ga, Ge is intentionally stabilized in the fcc structure [92]. Explicit computations of the nuclear wave function show that the double-well potentials are too shallow to localize the H in one of the wells, i.e., in one of the off-center configurations. Rather, the resulting nuclear wave function looks symmetric with the maximum at the center for all considered cases implying that the off-center configurations are dynamically unstable even at $T = 0$ K. In fact, as shown in Fig. 3, including zero-point vibrations the resulting H distribution function is symmetrically centered

TABLE I. DFT computed formation energies of interstitial H in various fcc metals. The first value in column one and two is the $T = 0$ K formation energy without including zero-point vibrations, the number in parentheses gives the energy change due to zero-point vibrations of H in the interstitial site and in the H_2 reference system (omission for H in OS in Au explained in Fig. 3). The interstitial site which has the lowest energy is the energetically preferred one and is shown in bold. Theoretical and experimental H interstitial formation volumes and preferential positions are shown in the last two columns. The literature data are taken from Refs. [93] (a), [94] (b), [95] (c), are derived from the solubility data in [96] (d), [97] (e), [98] (f), [99] (g), [100] (h), [101] (i), [102] (j), are derived from the solubility data in Refs. [103] (k), [104] (l), [105] (m), or are derived from the solubility data in [106] (n), [107–109] (o), [110] (p), [111] (q), [112,113] (r), [114] (s), [115] (t), [116] (u), [117] (v), [118] (w),[119] (x), [120] (y), high concentration (≈0.5) in [93] (z).

	E_f^{int} (eV)			H partial volume in Å^3		Interstitial position	
	DFT						
	OS (ZPE)	TS (ZPE)	Experiment	DFT	Experiment	DFT	Experiment
Ag	**0.71 (−0.09)**	0.71 (−0.02)	0.71[a], 0.72[a], 0.59[b] 0.64[c], 0.65[d]	2.19		OS	
Al	0.84 (−0.10)	**0.71 (−0.03)**	0.70[a], 0.71[e], 0.60[f], 0.65[e,d], 0.66[a,y], 0.67[g], 0.41[h], 0.84[i], 1.00[j]	4.82		TS	TS[t]
Au	0.91 (–)	**0.80 (−0.04)**	0.37[a], 0.33[d], 0.29[b], 0.21[k], 0.19[l], 0.74[a]	4.39		TS	
Ca	−0.58 (−0.10)	**−0.73 (−0.03)**	−0.78[m]	−0.41		TS	
Cu	**0.45 (−0.04)**	0.57 (0.04)	0.44[a], 0.60[n], 0.48[d], 0.38[n], 0.57[b]	2.43		OS	
Ir	**0.97 (−0.06)**	1.19 (0.04)	0.76[d], 0.84[a]	2.32		OS	
Ni	**0.05 (−0.02)**	0.29 (0.06)	0.16[o], 0.17[d], 0.13[p], 0.15[q]	2.31	2.20[a]	OS	OS[a]
Pb	1.05 (−0.13)	**0.93 (−0.08)**	1.27[z]	4.93		TS	
Pd	**−0.11 (−0.09)**	−0.09 (0.03)	−0.10[r,u], −0.07[d]	2.67	2.47[a]	OS	OS[u,v,w]
Pt	**0.50 (−0.12)**	0.45 (0.00)	0.48[a], 0.49[s]	3.67		OS	OS[x]
Rh	**0.19 (−0.04)**	0.45 (0.04)	0.28[d]	2.50	2.40[a]	OS	
Th	**−0.51 (−0.04)**	−0.37 (0.01)	−0.42[d]	1.89		OS	

and indistinguishable from the case where the PES does not show a double-well potential. This finding is in agreement with experiment [119], where interstitial H in Pt was found to reside in the center position of OS. The zero-point energy for H in OS in Au is higher than the barrier to escape from OS, therefore, H is completely unstable there and resides only in TS in Au.

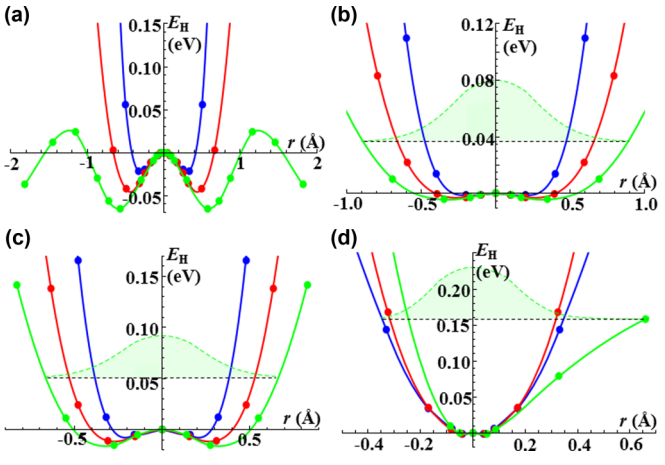

FIG. 3. (Color online) PES for H in OS in Au (a), in OS in Pb (b), in OS in Pt (c), and in TS in Ag (d) in different directions (blue line, ⟨100⟩; red line, ⟨110⟩; green line, ⟨111⟩) are shown by solid lines. The probability of finding a H atom is shown in the ⟨111⟩ direction by the dashed green line with the filling to the value of zero-point energy (shown by horizontal black dashed line). It is not shown for Au as the zero-point energy for H in OS in Au is higher than the barrier to escape and therefore H is completely unstable there.

As shown in Table I, the calculated H formation volume in those metals, for which the preferential position is OS, lies in a rather narrow range 2.2–2.7 Å^3 (except for Pt and Th), which has been often connected with an "incompressibility" of the dissolved H [122]. The result is in agreement with previous experimental studies of Baranowski *et al.* [122], who showed that the formation volume of interstitial H in some fcc metals and their alloys is about 2.8 Å^3 [123].

B. H-vacancy complexes

1. *Interstitial H close to a vacancy*

Since H binds in the vacancy to the nearest- and/or second-nearest-neighbor host atoms around the vacancy center, corresponding to an adsorption on the (vacancy) surface or subsurface, we consider in the following discussion the vacancy to be bounded by the planes formed by the first- and second-neighbor shell around the vacancy center (see Fig. 4). In the case of a perfect fcc lattice without relaxations, the vacancy has the form of an octahedron. Additionally, we also consider H solution in the interstitial sites that are situated closest to but not within the vacancy (the small octahedron and tetrahedron in Fig. 4). The compilation of the results in Fig. 5

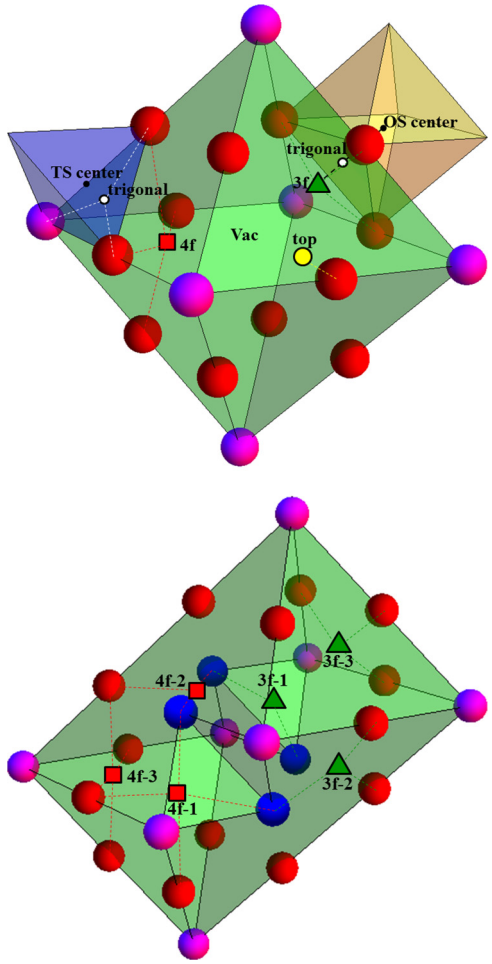

FIG. 4. (Color online) Visualization of relevant interstitial sites within a vacancy (top) and a divacancy (bottom) as well as the adjacent OS (brown) and TS (blue), host atoms from the first shell in red and in blue and from the second shell in magenta. The number of nearest-neighbor host metal atoms for atoms shown in magenta is 12, in red 11, in blue 10. H positions in 3f sites shown by green triangles, in 4f by red squares, in top by a yellow circle. The trigonal position in the $\{111\}$ plane is shown by a white dot and centers of OS or TS are marked by a black dot.

includes the corresponding formation energies at $\mu_{\mathrm{H}} = \mu_{\mathrm{H}}^{\mathrm{int},0}$. The same symbols as for regular bulk interstitial sites are used, but with lighter filling. The difference in the adjusted formation energies in both cases turned out to be small (a maximum value of about 0.1 eV was found for Al and Ir). Since the presence of a vacancy practically does not change the H formation energy in the nearby interstitial positions, a vacancy acts as a highly localized (short-range) trapping center for H in fcc metals.

2. *One H in a vacancy*

Binding energies of a H atom to a vacancy in different positions (from our DFT results and from experiment) are summarized in Table II and Fig. 5. Furthermore, for all metals considered here, H is not stable at the substitutional site (i.e., in the center of a vacancy), but is displaced in a specific direction. We have considered three different high-symmetry directions in this context (see Figs. 2 and 4): ⟨100⟩ (4f), ⟨110⟩ (top), and ⟨111⟩ (3f). We first determined the optimal distance of the H atom from the center of a vacancy for each of these directions. As a typical example, Fig. 6 shows the distance dependencies for Pd. We observe that H in the top position has the smallest optimal distance and at the same time the highest energy. This is a general finding for all studied fcc metals. In all considered cases, an intermediate displacement length is found for H in 3f positions (except for Al), and the largest displacement is observed for H in a 4f position. Due to the higher energy of the top position, the first H atom trapped by vacancies will be situated in a 3f and/or in a 4f position.

Experimental H positions from ion-channeling experiments are shown in Table III. For some metals, the observed configuration depends on the annealing temperature. Reasons are high-temperature effects on H mobility in fcc metals and the preference of different H positions inside a vacancy compared to the bulk crystal. When H is implanted in metals, it creates defects (e.g., self-interstitial host atoms and vacancies). At cryogenic temperatures, the mobility of H is suppressed and therefore most H atoms are located in bulk interstitial sites. In most fcc metals (Ag, Cu, Ni, Pd, Pt), this corresponds to OS and in Al to TS in perfect agreement with our DFT results (see Table I).

After annealing the system at higher temperature, H becomes mobile and will be eventually trapped in defects. This change in interstitial position is observed in ion-channeling experiments as for example for Pd (at higher than 90 K) and for Pt (at higher than 70 K). According to our results, H is located in OS in bulk but binds in a vacancy stronger to the 3f site compared to the 4f site in a vacancy for both of these metals. These findings nicely explain the experimentally observed change of the H position. The computed H behavior in Ir and Rh is similar to Pd and Pt so we expect that ion-channeling experiments on these metals will provide the same picture. In Ag, Al, Cu, and Ni hydrogen prefers the same interstitial type in the bulk and in the vacancy again in perfect agreement with experiments (see Table III).

At even higher temperature, H can be delocalized in a vacancy (so it can occupy both configurations 3f and 4f) if the binding energy in both sites is similar. Experimentally, this is observed for Cu, Ni, and Pd. Our DFT calculations show indeed almost degenerate binding energies for 3f and 4f sites for these metals (see Table II).

The H binding energy to a vacancy ranges in our study from 0.17 to 0.86 eV (see Table II), meaning that vacancies in the host lattice strongly trap H in fcc metals. Experimentally, several ranges of binding energies have been reported. For example, for Cu and Ni, two distinct ranges of binding energies have been observed in several studies: 0.19–0.26 eV [3,93,131] and 0.36–0.42 eV [3,131,132] in Cu, 0.24–0.28 eV [3,68,93,133,134] and 0.43–0.45 eV [3,68,133–135] in Ni. Several models were proposed to explain these two states. Initially, Norskov *et al.* [141] suggested that the site with the weakest binding energy (≈0.23 eV for Cu and ≈0.24 eV for Ni) corresponds to a H atom trapped by a self-interstitial host atom and the binding energy of ≈0.43 eV corresponds to a H atom inside a vacancy. Later, the same group provided an alternative explanation [70]: Employing an effective-medium theory, they observed that the first two H atoms can go into the positions inside a vacancy that provide optimal charge

TABLE II. Calculated binding energy (E_b) of a H atom to a vacancy and a divacancy in different positions. The H binding energy to a surface (see explanation in text) is derived using results of Ref. [124]. Experimental ranges for binding energies are shown in the last column. The experimental data are taken from Refs. [93] (a), [125] (b), [126] (c), [127] (d), [128] (e), [129] (f), [130] (g), [3] (h), [131] (i), [132] (j), [133] (k), [134] (l), [68] (m), [135] (n), [136] (o), [137] (p), [138] (q), [139] (r), [115] (s), [119] (t).

	DFT												
	Vacancy				Divacancy						Surface		
	Center	4f	3f	Top	4f-1	4f-2	4f-3	3f-1	3f-2	3f-3	4f	3f (fcc)	Experiment
Ag	−0.67	**0.23**	0.21	−0.01	0.25	**0.38**	0.19	0.18	0.24	0.18		0.55	≈0.45[b]
Al	−0.54	0.08	**0.25**	0.03	0.25	0.35	0.23	**0.67**	0.45	0.48			0.43±0.07[c], 0.53±0.03[d], 0.52±0.10[e], 0.71[f]
Au	−1.03	0.09	**0.29**	−0.002	**0.58**	0.45	0.23	0.57	0.46	0.42		0.70	≈0.6[g]
Ca	−1.58	−0.03	−0.23	−0.32	0.10	**0.39**	0.14	−0.52	−0.06	−0.11			
Cu	−0.54	**0.26**	0.20	0.04	0.28	**0.41**	0.21	0.16	0.25	0.18	0.53	**0.62**	0.19–0.26[h], 0.22[i], 0.23[a] 0.36–0.37[h], ⩾0.4[j], 0.42[i]
Ir	−0.49	0.63	**0.86**	0.62		0.98	0.69	**1.33**	0.94	0.86			
Ni	−0.65	**0.22**	0.20	0.02	0.26	**0.35**	0.21	0.19	0.24	0.20	0.58	**0.71**	0.24[k,l], 0.28[m,h], 0.27[a] 0.43[k,l], 0.44[m,n], 0.45[h], 0.58[o], 0.57±0.04[p]
Pb	−0.63	0.07	**0.17**	−0.05	0.17	**0.40**	0.18	**0.40**	0.29	0.28			
Pd	−1.00	0.16	**0.20**	−0.04	0.16	**0.28**	0.16	0.23	0.23	0.22	0.42	**0.49**	0.23[q,r], 0.15[q], 0.31[a]
Pt	−0.98	0.34	**0.57**	0.33	0.39	0.71	0.56	**0.83**	0.56	0.58		0.94	≈0.5[b]
Rh	−0.64	0.32	**0.35**	0.18	0.39	0.48	0.34	**0.49**	0.41	0.38	**0.79**	0.72	
Th	−1.08	**0.17**	-0.06	−0.42	0.14	0.20	0.12	−0.21	−0.04	−0.08			

density and thus maximize their binding energies. Increasing the number of H atoms introduces additional charge density on H sites that reduces H-vacancy binding energies.

The suggestion of Norskov *et al*. has been questioned by Fukai *et al*. [3], who carried out thermal desorption spectroscopy (TDS) experiments on H in electrodeposited Ni and Cu samples and in samples heat treated under high hydrogen pressures and high temperatures. Based on these experiments, they observed the formation of superabundant vacancies and two types of peaks, which they attributed to H trapped inside a vacancy. The low-temperature peak (corresponding to lower, i.e., energetically less favorable, binding energies) has been observed in all samples (heat treated, electrolytic, and electrodeposited) and in both materials. However, the appearance of the high-temperature peak (corresponding to a configuration with higher binding energy) was rather variable and its magnitude was noticeably higher in Ni than in Cu. Further, the position of the high-temperature peak depended on sample preparation and decomposed for Ni sometimes into two peaks. Based on these observations, Fukai *et al*. suggested as an alternative explanation that the lower binding energies (≈0.23 eV) in both metals correspond to H trapping inside a single vacancy, whereas the higher binding energies (≈0.43 eV) correspond to H trapped by divacancies.

To test this hypothesis, we performed calculations of H in a vacancy and a divacancy. According to our calculations, the trapping energy of the first H atom in a vacancy is 0.26 and 0.22 eV in Cu and Ni, respectively. This is in perfect agreement with the first experimental range of H binding energies [3,68,93,131,133,134]. Moreover, as H is not situated in the center of a vacancy, its binding is mostly dominated by the interaction with only the neighboring metal atoms at the internal surface of the vacancy.

Using the adsorption energies reported in a recent DFT study of H on transition-metal surfaces [124], which have been included in Table II, allows us to compare the adsorption of H in a vacancy (which can be considered as adsorbing H on an inner surface) and on a free surface. To make this comparison, we note that the 3f site on the inner surface is structurally similar to the fcc site on the (111) surface and the 4f vacancy site is similar to the 4f site on (100). The comparison of the values in Table II reveals that the binding energies of H to the free surface are not only systematically higher, but also the energetic order is different from the ones to the internal surface of a vacancy. For Cu and Ni, H inside a vacancy prefers the 4f site, whereas at the surface it prefers the 3f site on (111). For Rh, the opposite situation is observed.

This clear difference of what sites are preferred on the inner and outer surfaces can be understood by analyzing the configuration of the nearest-neighbor metal atoms to which the H atom is bound. The coordination number of the metal atoms at the inner surface of the vacancy is 11 (i.e., only one atom less than in bulk). Metal atoms situated at the free surface, however, have a much lower coordination [on the (111) surface nine atoms, on (001) eight atoms], yielding a higher reactivity and a stronger H trapping. Based on this argument, the affinity of a site to trap H is expected to correlate inversely to the coordination number of the metal atoms surrounding this site.

To confirm this hypothesis and to explain different experimental binding energies reported in the literature, we calculated also the binding of a H atom to a divacancy. There are three variants of 3f and 4f sites inside a divacancy (see

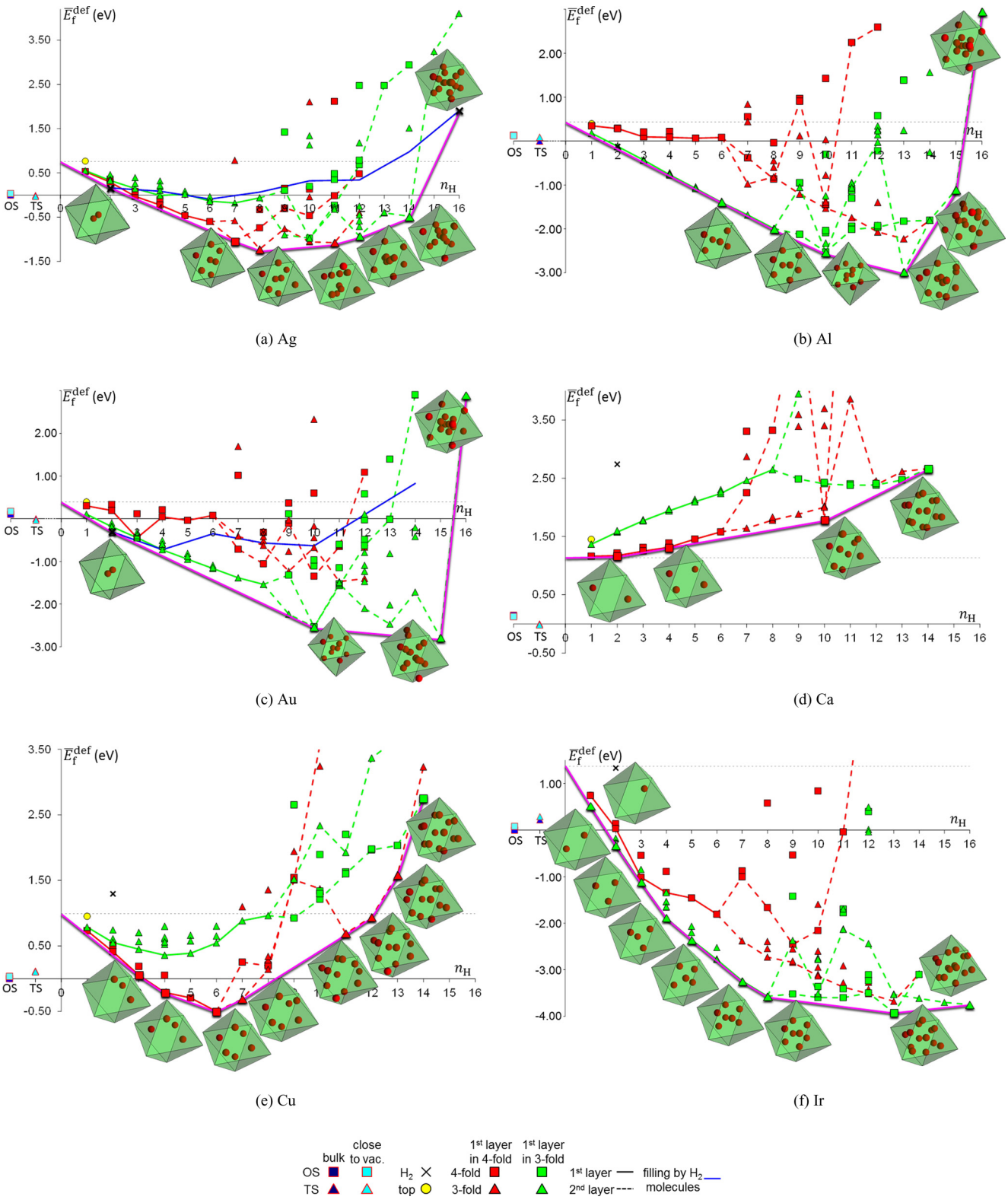

FIG. 5. (Color online) H-adjusted energy of formation [see Eq. (6)] in bulk OS and 4f vacancy positions (indicated by squares), TS and 3f positions (triangles), top vacancy positions (circles), and the formation of H_2 molecules (crosses). Results for H outside a vacancy are shown for bulk interstitial sites (blue/dark symbols) and interstitial sites close to an empty vacancy (light blue). Results for H inside a vacancy are shown with the number of incorporated H atoms. Additionally, stable H-vacancy complexes for a fixed number of H atoms with only one H layer (solid line) and with a second layer (dashed line) are indicated. The color of lines and symbols (triangles or squares) shows the type of filling in the first layer: green, H in 3f sites; red, H in 4f sites. The filling of vacancies by H_2 molecules is indicated for Ag, Au, and Pb by blue solid lines. The vacancy formation energy is shown by dashed black lines. The most stable H-vacancy complexes are the vertices on the convex hull indicated by magenta lines.

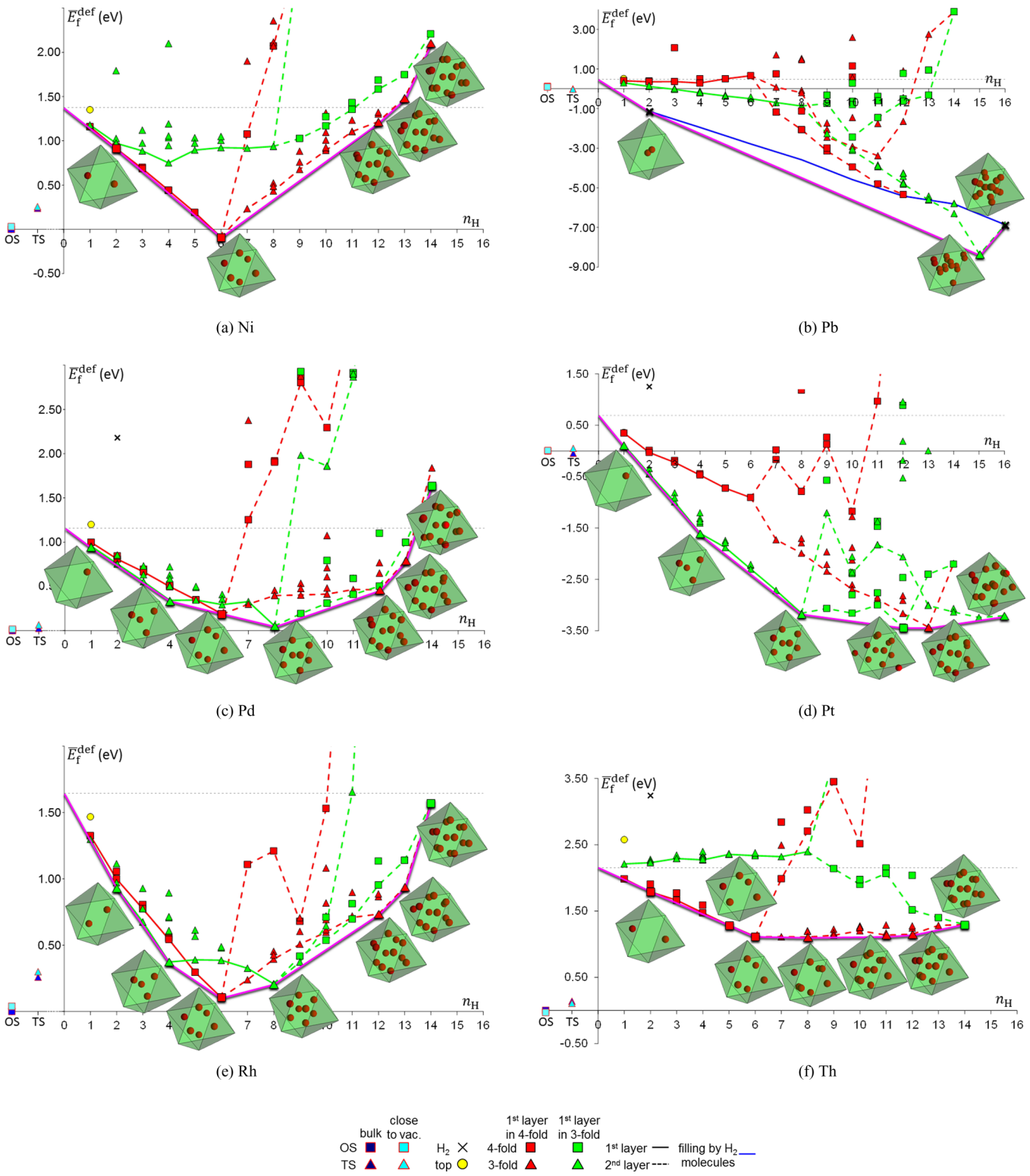

(a) Ni (b) Pb

(c) Pd (d) Pt

(e) Rh (f) Th

FIG. 5. (Color online) H adjusted energies of formation (continued).

Fig. 4 bottom). The H binding energies in these positions are also provided in Table II. They are systematically higher than for the monovacancy, but lower than at the free surface. The most preferable position in the divacancy is for all elements either the 4f-2 or the 3f-1 site. In both positions, the H atom is bound to two low-coordinated metal atoms. All these findings corroborate the above hypothesis of an inverse correlation between H binding and coordination number of the neighboring metal atoms.

Based on these results, we can now explain the experimentally observed ranges of H trapping energies. Reported H binding energies

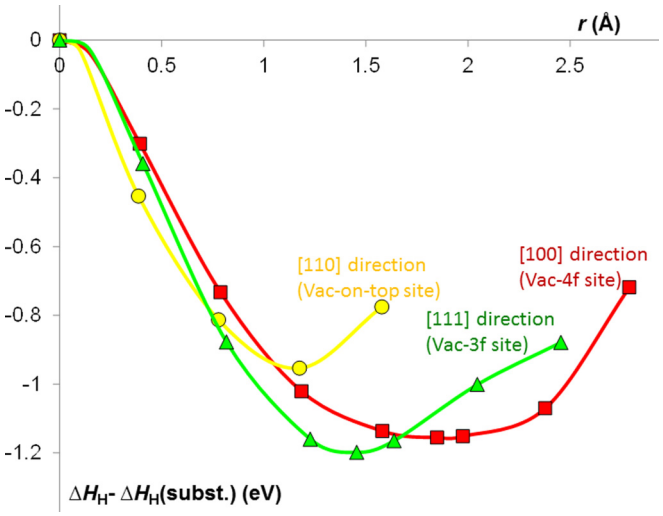

FIG. 6. (Color online) H energy in a vacancy in Pd when displaced in different directions from its center: red line, ⟨100⟩ direction; yellow line, ⟨110⟩; green line, ⟨111⟩.

(i) of 0.19–0.26 eV in Cu [3,93,131], 0.24–0.28 eV in Ni [3,68,93,133,134], 0.15 and 0.23 eV in Pd [138,138,139], about 0.5 eV in Pt [125] correspond to H trapping in monovacancies;

(ii) of 0.6 eV in Au [130], of 0.36–0.42 eV in Cu [3,131,132], of 0.43–0.45 eV in Ni [3,68,133–135], of 0.31 eV in Pd [93] correspond to H trapped in divacancies;

TABLE III. Most preferable position of a single H atom in fcc metals. The displacement from the ideal interstitial sites when H enters a vacancy is given for theory and experiments in Å (positive value, displacement towards center of vacancy). Experimentally observed H partial occupancies of interstitial sites are given in percent in the last column. The experimental data depend on the annealing temperature given in parentheses and are taken from Refs. [125] (a), [115] (b), [131] (c), [134] (d), [139] (e), [119] (f), [140] (g).

	DFT		Experimental
	Position	displacement	location
Ag	4f	−0.01	OS (25–320 K)[a]
Al	3f	0.20	TS (25–180 K)[b]
Au	3f	0.08	
Ca	4f	−0.29	
Cu	4f	0.08	OS(25–300 K)[a], OS(25–75 K)[c] 82%: 0.3 Å from OS to Vac and 18%: 0.2 Å from TS to Vac (273 K)[c]
Ir	3f	0.39	
Ni	4f	0.18	OS(25–250 K)[g], OS (25 K)[d] 87%: 0.3 Å from OS to Vac and 13%: 0.2 Å from TS to Vac (270 K)[d]
Pb	3f	0.07	
Pd	3f	0.25	OS (25–90 K), TS (90–180 K)[a] 37%: 0.2 Å from OS to Vac and 63%: 0.15 Å from TS to Vac (190 K)[e]
Pt	3f	0.29	OS(25–70 K), TS (70–275 K)[f]
Rh	3f	0.39	
Th	4f	−0.10	

(iii) of 0.36–0.62 eV in Al [126–128] represent an overlap of binding energies from trapping in vacancies and divacancies;

(iv) of about 0.45 eV in Ag [125], of 0.71 eV in Al [129], of 0.53–0.61 in Ni [136,137] correspond to H trapping on the internal surfaces of voids or bubbles.

3. *Formation of H_2 molecules in a vacancy*

The formation of H_2 molecules in pores of crystalline material is in some theoretical models considered as the key process to explain hydrogen embrittlement. To investigate this mechanism in the context of vacancies, we carefully studied the possibility of hydrogen molecule formation. For this purpose, the initial distance of two hydrogen atoms within a single vacancy was reduced to the H-H bond length of a H_2 molecule in vacuum ($d_{\text{H-H}}$ =0.74 Å). We have calculated the energetics of this pair of H atoms at different positions and with different orientations within a vacancy allowing relaxations of atoms.

In Ni and Rh, two H atoms never stay together, but rather dissociate into H atoms bounded to the internal vacancy surface. Therefore, in these metals a H_2 molecule in a single vacancy is unstable. We also observed the similar instability of a H_2 molecule in the vacancy of fcc Fe [142]. For other fcc metals, the distance between two H atoms changed only slightly and the atoms stayed coupled to each other. This indicates that metastable H_2 molecules can be formed in vacancies. The bond length between these H atoms is between 0.72 and 1.00 Å. To understand whether such a configuration can also be thermodynamically stable we compared in detail their energy with the energy of any other configuration containing two H atoms (see Fig. 5). It turned out that in Ag, Au, and Pb, a H_2 molecule is stable in a vacancy. In Al the formation energy of a H_2 molecule is equal to that of placing two H atoms on the 3f sites inside a vacancy. Since not only a single but several H_2 molecules can form in a vacancy, we studied also the formation of multiple H_2 molecules in a single vacancy. These calculations were restricted to Ag, Au, and Pb, i.e., to metals where the formation of a H_2 molecule was found to be more preferable than any other distribution of two H atoms in a vacancy.

For Au, only the first H_2 molecule is thermodynamically more stable than other distributions of the H atoms. For Ag, also eight H_2 molecules can be formed and are stable against dissociation. For Pb, practically for all levels of vacancy filling H_2 molecules are more stable than any configuration of isolated H atoms.

4. *First H layer in a vacancy*

Next, we have studied the formation of a first layer of H atoms on the inner surface. We perform our calculations starting from configurations for which H atoms in one layer occupy the same type of positions. Accordingly, up to six H atoms can decorate a vacancy in 4f positions and up to eight H atoms in 3f positions. The corresponding symbols for the adjusted formation energies (squares for 4f sites and triangles for 3f sites) are connected by solid lines in Fig. 5. We did not consider on-top positions since for all studied metals this site has been found to be energetically less favorable than both the 3f and the 4f sites.

As shown in Fig. 5, for most metals the adsorption energy for H on the 3f or 4f sites increases linearly with the number of H atoms implying that effects due to H-H interaction (which would result into a nonlinear dependence) are small and in most cases negligible. Thus, H atoms have only little impact on host atoms that are further away, binding to other H atoms. This is an additional result that shows that the two experimentally observed H adsorption bands can not be explained by varying the number of H atoms in a vacancy (see also the discussion in Sec. III B 2).

Finally, a sequential filling of the 4f sites (with up to six H atoms) is observed in Cu, Ni, Th, and of the threefold sites (with up to eight H atoms) in Al, Ir, Pt. In Ag and Au, the sequential filling of 4f sites and 3f sites, respectively, is interrupted by the formation of a single H_2 molecule, which is more stable than any other configuration of two H atoms. In Pd and Rh, vacancies start to trap H atoms in 3f sites, at higher filling in 4f sites, but at even higher fillings they switch again back to 3f sites. Vacancies in Pb will be filled mostly with H_2 molecules only.

5. Second H layer in a vacancy

We have also studied the possibility of forming a second layer of H atoms inside a vacancy. The second layer starts with the seventh (ninth) H atom, if the occupied sites of the first layer were of 4f (3f) type. The first H atom in the second layer can again go to the 3f (triangle in Fig. 2) and 4f (square) sides.

In contrast to the first layer, the H formation energies in the second layer are rather scattered because of the variety of different configurations. First, the atoms of the second H layer do not necessarily have to be inside the volume formed by the atoms of the first H layer (cube for 3f sites or octahedron for 4f sites), i.e., they do not need to be closer to the center of the vacancy. Such a change of stacking order can occur if the H position for the second layer is different from the first one (i.e., 3f versus 4f sites). It turns out that such a change is preferred for all considered fcc metals. However, it does not remain the most stable one for the complete filling of the second layer in Ag, Au, and Pb as discussed in the following.

One of the reasons is the formation of H_2 molecules. This occurs in Ag, Au, and Pb, where H atoms of the second layer form H_2 molecules with each other or with the atoms of the first layer. A second general observation that applies to all metals is that the H formation energy for second layer atoms in fourfold positions decreases if also the first layer atoms are in fourfold positions. The reason is that the latter are pushed outside the first shell of host atoms (shown by red balls in Fig. 4). We still consider this space as being attributed to a vacancy. This situation occurs in all studied metals for different configurations. A similar repulsion can also be observed if both H layers are in 3f positions as, for example, in Ca, Ni, Pd, and Rh at very large H pressures. However, we do not consider these situations since the H atoms of the first layer move in this case to OS close (but not inside) a vacancy via a trigonal site (along the dashed black line in Fig. 4).

6. Stable H-vacancy complexes

A key question of the current paper is to identify the thermodynamically stable H-vacancy complexes, i.e., complexes that can be formed under thermodynamic equilibrium conditions and that are stable against the formation of other defects. At $T = 0$ K, these structures are given by the kinks on the convex hull and their respective structures are shown in Fig. 5 by the green box filled with H atoms marked by red balls. If the number of H atoms per vacancy lies in the range between two vertices, both corresponding H-vacancy complexes will occur in the system with probabilities that follow a lever rule. The description used so far, where we plotted the energy as a function of the number of H atoms, corresponds to a canonical ensemble.

In the following, we will transfer our results to a grand canonical description where not the number of H atoms is fixed, but the H chemical potential μ_H. This description allows us to directly connect to experiment, where temperature and partial pressure (or overpotential in electrochemical experiments) that determine μ_H, rather than the number of H atoms, are controlled.

We therefore plot the formation energies of H-vacancy complexes as a function of μ_H, according to Eq. (2) (see Fig. 7). To relate the H chemical potential to experimentally directly accessible and controllable quantities, we also show the corresponding H partial pressures at 300 K on the same axis [93]. The red line on these figures represents the H-vacancy complexes with the lowest energy of formation (i.e., the thermodynamically stable complexes that form the convex hull) for a given H chemical potential.

The blue lines in Fig. 7 indicate the number of H atoms in a vacancy as a function of the H chemical potential. Steps along the blue line separate the ranges of μ_H, where the same H-vacancy complex is stable. These complexes are identical with the complexes forming the convex hull in Fig. 5. At $T = 0$ K, only one type of H-vacancy complex can be the most stable at a fixed H chemical potential, while up to two H-vacancy complexes can be the most stable at a fixed number of H atoms per vacancy. Using the blue line in Fig. 7, we can readily relate the number of H atoms per vacancy to a H chemical potential. For a low-H chemical potential, empty vacancies are dominant, while with increasing μ_H the number of H atoms in the most stable H-vacancy complexes also increases.

As explained in the context of Eq. (3), the solution of H atoms inside a monovacancy is restricted to those H chemical potentials, for which no phase transformations into a hydride phase occurs. Therefore, the maximal number of H atoms inside a monovacancy is achieved at the H chemical potential corresponding to phase transformation into hydride phase.

To obtain this critical H chemical potential, we performed DFT calculations of different hydrides using the crystallographic structures known from experiment. Their formation energy per H atom given in Table IV is equal to the H chemical potential for the transformation into this hydride phase from a pure fcc bulk metal within a H atmosphere. According to our results, non-fcc-based types of hydrides for Al, Ca, and Th have the formation energies lower than the μ_H for H to be trapped in a vacancy. Therefore, these metals are transformed into a hydride phase, before H enters the vacancy. Thus, vacancy filling with H is not relevant for Al, Ca, and Th.

According to our DFT calculations, for all other metals H goes into vacancies at H chemical potentials that are below

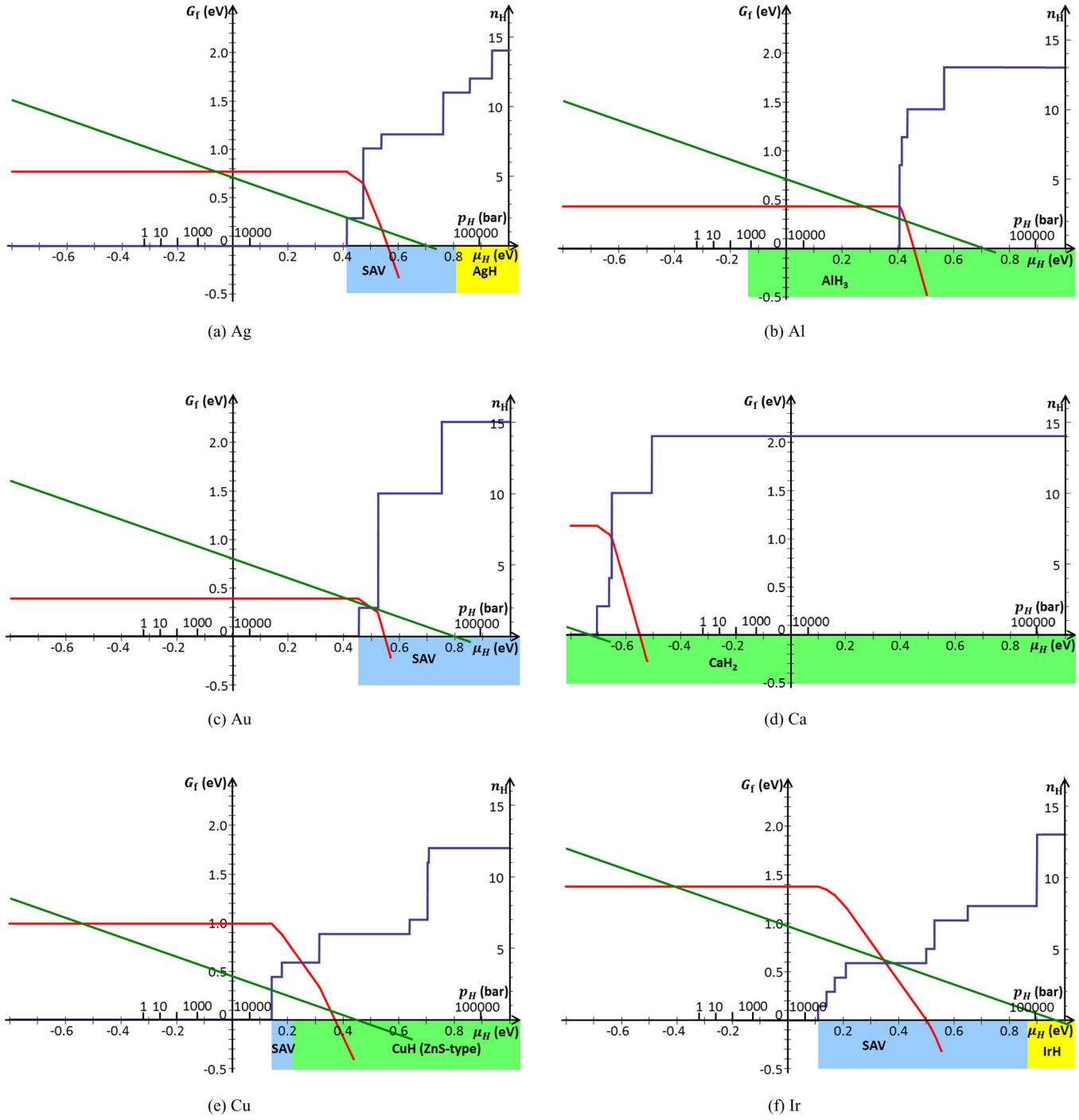

(a) Ag (b) Al

(c) Au (d) Ca

(e) Cu (f) Ir

FIG. 7. (Color online) Defect formation energies of interstitial H (green lines), thermodynamically stable H-vacancy complexes (red lines), and the number of H atoms in them (blue lines) as a function of H chemical potential (the corresponding H partial pressure at 300 K is given in bars). The phase stability regions at 0 K are shown at the bottom: light blue, superabundant vacancy formation; yellow, NaCl type of hydride; green, other types of hydrides (not based on the fcc structure).

the critical value at which hydride formation starts. For most of the fcc metals, the chemical potential of NaCl type of hydride formation is very close to the H formation energy in an interstitial site implying that the H-H interaction is weak. In fact, it deviates by less than 0.1 eV for Ag, Ir, Pb, Pd, Pt, and Rh. For Au with $\mu_{\mathrm{H}}^{\mathrm{fcc}\rightarrow\mathrm{NaCl\text{-}hydr}} = 1.27$ eV (not shown) and Ni with $\mu_{\mathrm{H}}^{\mathrm{fcc}\rightarrow\mathrm{NaCl\text{-}hydr}} = -0.12$ eV it is larger. In Ni, this is primarily related to the change of the magnetic structure: Ni with a low-H concentration is ferromagnetic, while Ni hydride is nonmagnetic.

We give also the maximal number of H atoms in a monovacancy in fcc metals: Ag, 11; Au, 15; Ir, 8; Ni, 6; Pb, 15; Pd, 8; Pt, 13; Rh, 6. We should notice that the formation energies of H-vacancy complexes become zero at H chemical potentials smaller than that of a transformation into a new hydride phase for Ag, Au, Ir, Pb, Pt. This could

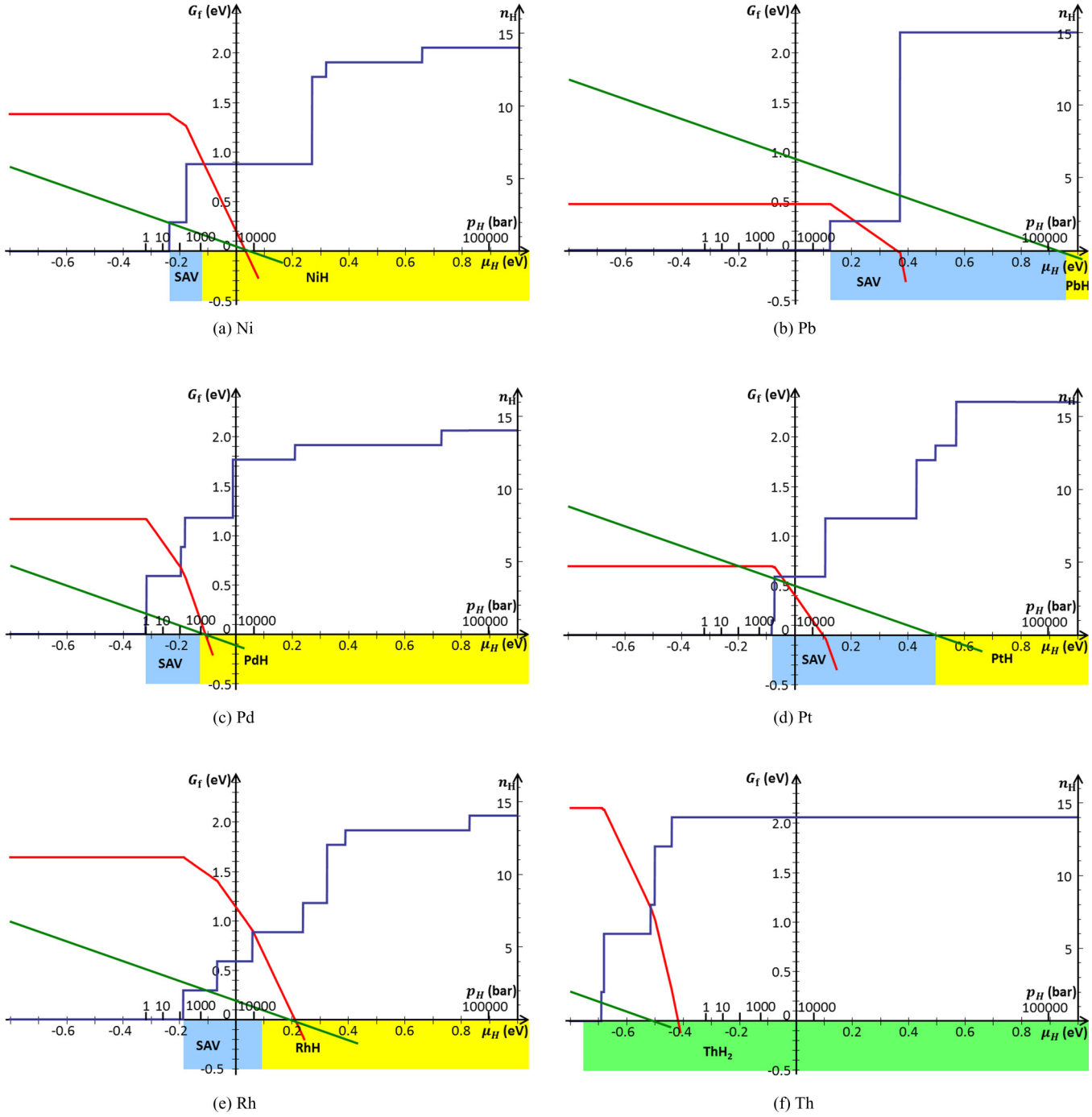

(a) Ni (b) Pb

(c) Pd (d) Pt

(e) Rh (f) Th

FIG. 7. (Color online) Defect formation energies (continued).

result into a formation of a vacancy-ordered phase in these metals. To investigate this possibility theoretically, this study would need to be extended to include the formation energies of vacancy-ordered phases with different H filling.

7. *Superabundant vacancy formation*

The transition from empty to filled vacancies is accompanied by a decrease in the defect formation energy. Increasing the H chemical potential above this critical point ($\mu_{\mathrm{H}}^{\mathrm{SAV}}$) will thus result in a significant increase of the total vacancy concentration. These regions of superabundant vacancy formation are indicated by light blue rectangular-shaped boxes in Fig. 7. For Ni, Pd, Pt, Rh, this transition occurs below $\mu_{\mathrm{H}} = 0$ eV. This signifies that at low temperatures most vacancies in these metals are filled with H. They therefore have a significantly reduced formation enthalpy and this reduced value determines also the (thermodynamic) vacancy concentration.

According to our results, the lowest H chemical potential for SAV formation is found for Ni and Pd (-0.23 and -0.32 eV, respectively). These are the metals where SAV have been first detected experimentally at temperatures above 1000 K and in the GPa range of H pressures.

TABLE IV. Calculated formation energies of NaCl-type hydrides (space group Fm-$3m$) and non-fcc-based types of hydrides that have been observed in experiment.

Unit formula	Space group	Formation energy (eV/H atom)
AgH	Fm-$3m$	0.81
AlH	Fm-$3m$	0.78
AlH_2	Fm-$3m$	0.83
AlH_3	R-$3ch$	−0.14
AuH	Fm-$3m$	1.27
CaH	Fm-$3m$	−0.44
CaH_2	$Pnma$	−0.82
CuH	Fm-$3m$	0.46
CuH	$P6_3mc$	0.21
IrH	Fm-$3m$	0.86
NiH	Fm-$3m$	−0.12
Ni2H	$P3m1$	−0.06
PbH	Fm-$3m$	0.96
PdH	Fm-$3m$	−0.13
$PdH_{1.33}$	Pm-$3m$	0.18
$PdH_{1.33}$	P-$4m2$	0.02
PtH	Fm-$3m$	0.50
RhH	Fm-$3m$	0.09
ThH	Fm-$3m$	−0.53
ThH_2	$I4/mmm$	−0.75

Other metals with a low μ_H^{SAV} are Pt ($\mu_H^{SAV} = -0.08$ eV) and Rh ($\mu_H^{SAV} = -0.18$ eV), which would be good candidates for SAV detection. We should, however, notice that although the formation of Pt and Rh hydrides is endothermic at normal conditions, it becomes exothermic under pressure, as shown recently by DFT calculations [143,144] and by experiment for Rh [144]. Therefore, Pt and Rh hydride phases could compete with the SAV phase at high-H_2 pressures. To explore this possibility theoretically, this study would have to be extended to include the pressure dependence of defect energies and bulk hydrides.

Another three metals with possible SAV formation are Cu, Ir, and Pb (μ_H^{SAV}=0.14, 0.11 and 0.13 eV, respectively). Using TDS measurements, SAV formation has been suggested for Cu in H_2 atmosphere at 900 °C and 5 GPa. Although the same H-rich conditions should result in SAV formation in Pb, a detection would be difficult due to the low melting temperature of Pb. We should notice that although the H chemical potential for SAV formation is higher for Ag and Au (0.42 and 0.46 eV, respectively), it is still accessible in high-pressure H_2 atmosphere or in electrochemical experiments.

IV. CONCLUSIONS

Using density functional theory, the solubility of H in the bulk phase and its interaction with vacancies was investigated in 12 fcc metals. Unlike the common belief that H occupies octahedral sites in fcc metals, we find that tetrahedral sites are preferred in Al, Au, Ca, and Pb. We further clarify that zero-point vibrations are important for the energetics and the geometry of H in interstitial sites.

Our results show that vacancies strongly trap H in all considered fcc metals (except of Ca). This affinity to trap H is spatially highly localized; already the interstitial sites nearest to the vacancy show a H solvation energy that is almost indistinguishable from the corresponding bulk value. Thus, vacancies are effective, but spatially very short-ranged trapping centers for H in fcc metals. We further find that H is stronger bound to divacancies and even stronger to surfaces. As a reason for these different H affinities, we identified an inverse correlation between the ability of a host atom to bind a H atom and its coordination number, i.e., to the number of nearest-neighbor host atoms. For an atom in the free surface, this number is smaller than for an atom in the inner surface of a vacancy, explaining the stronger binding of a H atom to the surface compared to the vacancy. The existence of these various defect structures could explain different experimental ranges for binding energies.

Based on the detailed thermodynamic analysis, we derive rigorous conditions for the maximal number of H atoms that can be trapped by a single vacancy. Multiple H atoms inside a vacancy can form H_2 molecules in practically all studied metals (except of Ni and Rh), but they are thermodynamically stable only in Ag, Au, and Pb.

The necessary conditions to form superabundant vacancies is derived. Using this condition, we show that in practically all investigated metals (except Al, Ca, and Th), superabundant vacancy formation is possible in a H-rich atmosphere before the metals transform into a hydride phase.

This study provides a complete thermodynamic analysis of H interaction with vacancies and may be used to investigate interaction of other light interstitial elements with vacancies or other point defects.

ACKNOWLEDGMENTS

We thank Y. Fukai for fruitful discussions and comments. We acknowledge funding by the Interdisciplinary Center for Materials Simulation (ICAMS), which is supported by ThyssenKrupp AG, Bayer MaterialScience AG, Salzgitter Mannesmann Forschung GmbH, Robert Bosch GmbH, Benteler Stahl/Rohr GmbH, Bayer Technology Services GmbH, and the state of North-Rhine Westphalia, as well as the EU in the framework of the ERDF.

[1] Y. Fukai and N. Ōkuma, Phys. Rev. Lett. **73**, 1640 (1994).
[2] Y. Fukai and N. Ōkuma, Jpn. J. Appl. Phys., Part 2 **32**, L1256 (1993).
[3] Y. Fukai, M. Mizutani, S. Yokota, M. Kanazawa, Y. Miura, and T. Watanabe, J. Alloys Compd. **356**, 270 (2003).
[4] K. Nakamura and Y. Fukai, J. Alloys Compd. **231**, 46 (1995).

[5] D. dos Santos, S. Miraglia, and D. Fruchart, J. Alloys Compd. **291**, L1 (1999).
[6] Y. Fukai, Y. Ishii, T. Goto, and K. Watanabe, J. Alloys Compd. **313**, 121 (2000).
[7] K. Watanabe, N. Ōkuma, Y. Fukai, Y. Sakamoto, and Y.Hayashi, Scr. Mater. **34**, 551 (1996).
[8] K. Sakaki, R. Date, M. Mizuno, H. Araki, and Y. Shirai, Acta Mater. **54**, 4641 (2006).
[9] H. Birnbaum, C. Buckley, F. Zaides, E. Sirois, P. Rosenak, S. Spooner, and J. Lin, J. Alloys Compd. **253**, 260 (1997).
[10] Y. Fukai, T. Haraguchi, E. Hayashi, Y. Ishii, Y. Kurokawa, and J. Yanagawa, Defect Diffus. Forum **194**, 1063 (2001).
[11] Y. Fukai, K. Mori, and H. Shinomiya, J. Alloys Compd. **348**, 105 (2003).
[12] Y. Fukai, Y. Kurokawa, and H. Hiraoka, J. Jpn. Inst. Met. **61**, 663 (1997).
[13] Y. Fukai and M. Mizutani, Mater. Trans. **43**, 1079 (2002).
[14] Y. Fukai, Y. Shizuku, and Y. Kurokawa, J. Alloys Compd. **329**, 195 (2001).
[15] Y. Fukai, T. Hiroi, N. Mukaibo, and Y. Shimizu, J. Jpn. Inst. Met. **71**, 388 (2007).
[16] H. Koike, Y. Shizuku, A. Yazaki, and Y. Fukai, J. Phys.: Condens. Matter **16**, 1335 (2004).
[17] T. Iida, Y. Yamazaki, T. Kobayashi, Y. Iijima, and Y. Fukai, Acta Mater. **53**, 3083 (2005).
[18] J. Čížek, I. Procházka, F. Bečvář, R. Kužel, M. Cieslar, G. Brauer, W. Anwand, R. Kirchheim, and A. Pundt, Phys. Rev. B **69**, 224106 (2004).
[19] Y. Shirai, H. Araki, T. Mori, W. Nakamura, and K. Sakaki, J. Alloys Compd. **330**, 125 (2002).
[20] Y. Fukai and H. Sugimoto, J. Phys.: Condens. Matter **19**, 436201 (2007).
[21] V. Gavriljuk, V. Bugaev, Y. Petrov, A. Tarasenko, and B. Yanchitski, Scr. Mater. **34**, 903 (1996).
[22] Y. Yagodzinskyy, T. Saukkonen, S. Kilpelinen, F. Tuomisto, and H. Hnninen, Scr. Mater. **62**, 155 (2010).
[23] Y. Fukai, J. Alloys Compd. **356**, 263 (2003).
[24] Y. Fukai, Phys. Scr. **T103**, 11 (2003).
[25] S. Semiletov, R. Baranova, Y. Khodyrev, and R. Imamov, Kristallografiya **25**, 1162 (1980) [Sov. Phys.–Crystallogr. **25**, 665 (1980)].
[26] Y. Fukai, J. Alloys Compd. **231**, 35 (1995).
[27] S. Miraglia, D. Fruchart, E. Hlil, S. Tavares, and D. D. Santos, J. Alloys Compd. **317-318**, 77 (2001).
[28] Y. Fukai, *Computer Aided Innovation of New Materials* (Elsevier, Amsterdam, 1993), Vol. II, pp. 451–456.
[29] Y. Fukai, M. Yamakata, and T. Yagi, Z. Phys. Chem. **179**, 119 (1993).
[30] M. Nagumo, M. Takamura, and K. Takai, Metall. Mater. Trans. A **32**, 339 (2001).
[31] K. Sakaki, T. Kawase, M. Hirato, M. Mizuno, H. Araki, Y. Shirai, and M. Nagumo, Scr. Mater. **55**, 1031 (2006).
[32] Y. Z. Chen, G. Csiszár, J. Cizek, C. Borchers, T. Ungár, S. Goto, and R. Kirchheim, Scr. Mater. **64**, 390 (2011).
[33] Y. Shirai, F. Nakamura, M. Takeuchi, K. Watanabe, and M. Yamaguchi, in *Eighth International Conference on Positron Annihilation*, edited by V. Dorikens, M. Drikens, and D. Seegers (World Scientific, Singapore, 1989), p. 488.
[34] P. Chalermkarnnon, H. Araki, and Y. Shirai, Mater. Trans. JIM **43**, 1486 (2002).
[35] H. Noh, T. Flanagan, B. Corundero, and A. Craft, Scr. Metall. **25**, 225 (1991).
[36] H. Noh, T. Flanagan, and M. Ransick, Scr. Metall. **26**, 353 (1992).
[37] Y. Yamazaki, Y. Iijima, and M. Okada, Acta Mater. **52**, 1247 (2004).
[38] D. Fruchart, P. Chaudouet, R. Fruchart, A. Rouault, and J. Senateur, J. Solid State Chem. **51**, 246 (1984).
[39] H. Noh, J. Clewley, T. Flanagan, and A. Craft, J. Alloys Compd. **240**, 235 (1996).
[40] T. Flanagan, J. Clewley, H. Noh, J. Barker, and Y. Sakamoto, Acta Mater. **46**, 2173 (1998).
[41] H. Noh, T. Flanagan, and Y. Sakamoto, Scr. Metall. Mater. **29**, 445 (1993).
[42] V. Antonov, T. Antonova, I. Belash, E. Ponyatovskii, and V. Rashupkin, Phys. Status Solidi A **78**, 137 (1983).
[43] D. Sun, F. Gingl, Y. Nakamura, H. Enoki, M. Bououdina, and E. Akiba, J. Alloys Compd. **333**, 103 (2002).
[44] T. B. Flanagan and H. Noh, J. Alloys Compd. **231**, 1 (1995).
[45] T. Flanagan, A. Craft, T. Kuji, K. Baba, and Y. Sakamoto, Scr. Metall. **20**, 1745 (1986).
[46] K. Baba, Y. Niki, Y. Sakamoto, T. Flanagan, and A. Craft, Scr. Metall. **21**, 1147 (1987).
[47] S. Lee, T. Flanagan, and G. Kim, Scr. Metall. Mater. **32**, 827 (1995).
[48] S.-M. Lee, H. Noh, T. B. Flanagan, and S. Luo, J. Phys.: Condens. Matter **19**, 326222 (2007).
[49] T. Fujikawa, T. Yoshikawa, T. Ohnishi, and T. Sato, Jpn. J. Appl. Phys. **40**, 2191 (2001).
[50] Z. R. Xu and R. B. McLellan, Acta Mater. **46**, 4543 (1998).
[51] C. W. Tien, Ph.D. thesis, University of Illinois Urbana-Champaign, 1994.
[52] E. Hayashi, Y. Kurokawa, and Y. Fukai, Phys. Rev. Lett. **80**, 5588 (1998).
[53] K. Tanaka, H. Tanaka, and H. Kawaguchi, J. Alloys Compd. **330-332**, 256 (2002).
[54] K. Tanaka and K. Nagai, Mater. Trans. **43**, 2692 (2002).
[55] V. M. Sharapov, L. E. Gavrilov, V. S. Kulikauskas, and A. V. Markin, J. Nucl. Mater. **233-237**, 870 (1996).
[56] B. Zajec, V. Nemani, and C. Ruset, J. Nucl. Mater. **412**, 116 (2011).
[57] W. Möller, F. Besenbacher, and J. Bottiger, Appl. Phys. A **27**, 19 (1982).
[58] S. M. Myers, P. M. Richards, D. M. Follstaedt, and J. E. Schirber, Phys. Rev. B **43**, 9503 (1991).
[59] M. Iwamoto and Y. Fukai, Mater. Trans. **40**, 606 (1999).
[60] M. Nagumo, ISIJ Int. **41**, 590 (2001).
[61] K. Takai, H. Shoda, H. Suzuki, and M. Nagumo, Acta Mater. **56**, 5158 (2008).
[62] A. Cuitiño and M. Ortiz, Acta Mater. **44**, 427 (1996).
[63] H. Osono, T. Kino, Y. Kurokawa, and Y. Fukai, J. Alloys Compd. **231**, 41 (1995).
[64] I. Bernstein, Metall. Mater. Trans. **1**, 3143 (1970).
[65] B. Rath and I. Bernstein, Metall. Mater. Trans. B **2**, 2845 (1971).
[66] Q.-Z. Chen, W.-Y. Chu, Y.-B. Wang, and C.-M. Hsiao, Acta Metall. Mater. **43**, 4371 (1995).
[67] R. Nazarov, T. Hickel, and J. Neugebauer, Phys. Rev. B **82**, 224104 (2010).

[68] S. M. Myers, P. Nordlander, F. Besenbacher, and J. K. Nørskov, Phys. Rev. B **33**, 854 (1986).
[69] F. Besenbacher, S. Myers, P. Nordlander, and J. Nørskov, J. Appl. Phys. **61**, 1788 (1987).
[70] P. Nordlander, J. K. Nørskov, F. Besenbacher, and S. M. Myers, Phys. Rev. B **40**, 1990 (1989).
[71] Y.-L. Liu, Y. Zhang, H.-B. Zhou, G.-H. Lu, F. Liu, and G.-N. Luo, Phys. Rev. B **79**, 172103 (2009).
[72] D. F. Johnson and E. A. Carter, J. Mater. Res. **25**, 315 (2010).
[73] K. Heinola, T. Ahlgren, K. Nordlund, and J. Keinonen, Phys. Rev. B **82**, 094102 (2010).
[74] K. Ohsawa, J. Goto, M. Yamakami, M. Yamaguchi, and M. Yagi, Phys. Rev. B **82**, 184117 (2010).
[75] Y. Tateyama and T. Ohno, Phys. Rev. B **67**, 174105 (2003).
[76] K. Ohsawa, K. Eguchi, H. Watanabe, M. Yamaguchi, and M. Yagi, Phys. Rev. B **85**, 094102 (2012).
[77] G. Lu and E. Kaxiras, Phys. Rev. Lett. **94**, 155501 (2005).
[78] L. Ismer, M. S. Park, A. Janotti, and C. G. Van de Walle, Phys. Rev. B **80**, 184110 (2009).
[79] O. Y. Vekilova, D. I. Bazhanov, S. I. Simak, and I. A. Abrikosov, Phys. Rev. B **80**, 024101 (2009).
[80] P. Hohenberg and W. Kohn, Phys. Rev. **136**, B864 (1964).
[81] W. Kohn and L. J. Sham, Phys. Rev. **140**, A1133 (1965).
[82] G. Kresse and J. Hafner, Phys. Rev. B **48**, 13115 (1993).
[83] G. Kresse and J. Furthmüller, Phys. Rev. B **54**, 11169 (1996).
[84] G. Kresse and J. Furthmüller, Comput. Mater. Sci. **6**, 15 (1996).
[85] J. P. Perdew, *Electronic Structure of Solids* (Akademie Verlag, Berlin, 1991), p. 11.
[86] R. Nazarov, T. Hickel, and J. Neugebauer, Phys. Rev. B **85**, 144118 (2012).
[87] Energy cutoff for Ag is 270 eV; Al, 250 eV; Au, 270 eV; Ca, 270 eV; Cu, 290 eV; Ir, 220 eV; Ni, 350 eV; Pb, 200 eV; Pd, 280 eV; Pt, 250 eV; Rh, 250 eV; Th, 270 eV.
[88] M. Methfessel and A. T. Paxton, Phys. Rev. B **40**, 3616 (1989).
[89] R. Kirchheim, Acta Mater. **55**, 5129 (2007).
[90] P. Nordlander, S. Holloway, and J. Nørskov, Surf. Sci. **136**, 59 (1984).
[91] C. Wolverton, V. Ozoliņš, and M. Asta, Phys. Rev. B **69**, 144109 (2004).
[92] U. Aydin, L. Ismer, T. Hickel, and J. Neugebauer, Phys. Rev. B **85**, 155144 (2012).
[93] Y. Fukai, *The Metal-Hydrogen System*, 2nd ed. (Springer, Heidelberg, 2005).
[94] R. McLellan, J. Phys. Chem. Solids **34**, 1137 (1973).
[95] P. Subramanian, J. Phase Equilib. **12**, 649 (1991).
[96] E. Fromm and H. Jehn, Bull. Alloy Phase Diagrams **5**, 324 (1984).
[97] W. Eichenauer, Zeitschrift für Metallkunde **59**, 613 (1968).
[98] W. Eichenauer, K. Hattenbach, and A. Peblez, Zeitschrift für Metallkunde **52**, 682 (1961).
[99] R. A. Edwards and W. Eichenauer, Scr. Metall. **14**, 971 (1980).
[100] C. E. Ransley and H. Neufeld, J. Inst. Met. **74**, 599 (1948).
[101] W. Eichenauer and A. Pebler, Zeitschrift für Metallkunde **48**, 373 (1957).
[102] E. Hashimoto and T. Kino, J. Phys. F: Met. Phys. **13**, 1157 (1983).
[103] C. L. Thomas, Trans. AIME **239**, 485 (1967).
[104] W. Eichenauer and D. Liebscher, Z. Naturforsch. **17a**, 355 (1962).
[105] H. Lee, Metall. Mater. Trans. A **7**, 431 (1976).
[106] V. N. Verbetsky and S. V. Mitrokhin, Solid State Phenomena **73-75**, 503 (2000).
[107] W. M. Robertson, Zeitschrift für Metallkunde **64**, 436 (1973).
[108] Y. Ebisuzaki, W. J. Kass, and M. O'Keeffe, J. Chem. Phys. **46**, 1378 (1967).
[109] F. Jones and R. Pehlke, Metall. Mater. Trans. B **2**, 2655 (1971).
[110] W. Eichenauer, W. Löser, and H. Witte, Zeitschrift für Metallkunde **56**, 287 (1965).
[111] W. Eichenauer, Mem. Sci. Rev. Met. **57**, 943 (1960).
[112] P. T. Gallagher and W. A. Oates, Trans. AIME **245**, 179 (1969).
[113] F. Manchester, A. San-Martin, and J. Pitre, J. Phase Equilib. **15**, 62 (1994).
[114] *Gase und Kohlenstoff in Metallen*, edited by E. Fromm and E. Gebhardt (Springer, Berlin, 1976).
[115] J. P. Bugeat, A. C. Chami, and E. Ligeon, Phys. Lett. A **58**, 127 (1976).
[116] H. D. Carstanjen, J. Dünstl, G. Löbl, and R. Sizmann, Phys. Status Solidi A **45**, 529 (1978).
[117] J. M. Rowe, J. J. Rush, L. A. de Graaf, and G. A. Ferguson, Phys. Rev. Lett. **29**, 1250 (1972).
[118] K. Sköld and G. Nelin, J. Phys. Chem. Solids **28**, 2369 (1967).
[119] E. Ligeon, J. Bugeat, R. Danielou, J. Fontenille, and A. Guivarch, J. Radiol. Nucl. Chem. **55**, 367 (1980).
[120] M. Ichimura, H. Katsuta, Y. Sasajima, and M. Imabayashi, J. Phys. Chem. Solids **49**, 1259 (1988).
[121] J. Nørskov and F. Besenbacher, J. Less-Common Met. **130**, 475 (1987).
[122] B. Baranowski, S. Majchrzak, and T. B. Flanagan, J. Phys. F: Met. Phys. **1**, 258 (1971).
[123] R. Griessen, Phys. Rev. B **38**, 3690 (1988).
[124] P. Ferrin, S. Kandoi, A. U. Nilekar, and M. Mavrikakis, Surf. Sci. **606**, 679 (2012).
[125] J. P. Bugeat and E. Ligeon, Phys. Lett. A **71**, 93 (1979).
[126] S. Linderoth, Philos. Mag. Lett. **57**, 229 (1988).
[127] H. Rajainmäki, S. Linderoth, R. M. Nieminen, and H. E. Hansen, Mater. Sci. Forum **15-18**, 611 (1987).
[128] S. M. Myers, F. Besenbacher, and J. K. Nørskov, J. Appl. Phys. **58**, 1841 (1985).
[129] G. A. Young and J. R. Scully, Acta Mater. **46**, 6337 (1998).
[130] J. P. Bugeat and E. Ligeon, in Proceedings of the 2nd International Conference on Hydrogen in Metals, 1977 (unpublished).
[131] F. Besenbacher, B. B. Nielsen, and S. M. Myers, J. Appl. Phys. **56**, 3384 (1984).
[132] B. Lengeler, S. Mantl, and W. Triftshauser, J. Phys. F: Met. Phys. **8**, 1691 (1978).
[133] F. Besenbacher, J. Bøttiger, and S. M. Myers, J. Appl. Phys. **53**, 3536 (1982).
[134] F. Besenbacher, H. Bogh, A. A. Pisarev, M. J. Puska, S. Holloway, and J. K. Nørskov, Nucl. Instrum. Methods Phys. Res., Sec. B **4**, 374 (1984).
[135] C. Szeles and A. Vertes, J. Phys. F: Met. Phys. **17**, 2031 (1987).
[136] S. Linderoth, H. Rajainmäki, and R. M. Nieminen, Phys. Rev. B **35**, 5524 (1987).
[137] H. Rajainmäki, S. Linderoth, H. E. Hansen, and R. M. Nieminen, J. Phys. F: Met. Phys. **18**, 1109 (1988).

[138] S. Myers, W. Wampler, F. Besenbacher, S. Robinson, and N. Moody, Mater. Sci. Eng. **69**, 397 (1985).
[139] F. Besenbacher, S. M. Myers, and J. K. Nørskov, Nucl. Instrum. Methods Phys. Res., Sec. B **7-8**, 55 (1985).
[140] J. Mory and E. Ligeon, J. Mater. Sci. **17**, 925 (1982).
[141] J. K. Nørskov, F. Besenbacher, J. Bøttiger, B. B. Nielsen, and A. A. Pisarev, Phys. Rev. Lett. **49**, 1420 (1982).
[142] R. Nazarov, T. Hickel, and J. Neugebauer (unpublished).
[143] D. Y. Kim, R. H. Scheicher, C. J. Pickard, R. J. Needs, and R. Ahuja, Phys. Rev. Lett. **107**, 117002 (2011).
[144] B. Li, Y. Ding, D. Y. Kim, R. Ahuja, G. Zou, and H.-K. Mao, Proc. Natl. Acad. Sci. USA **108**, 18618 (2011).